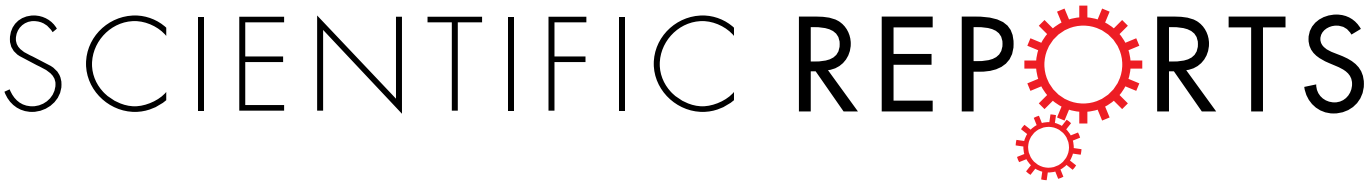

OPEN

Optical forces in nanorod metamaterial

Andrey A. Bogdanov[1,2,3], Alexander S. Shalin[1] & Pavel Ginzburg[4]

Received: 24 July 2015
Accepted: 29 September 2015
Published: 30 October 2015

Optomechanical manipulation of micro and nano-scale objects with laser beams finds use in a large span of multidisciplinary applications. Auxiliary nanostructuring could substantially improve performances of classical optical tweezers by means of spatial localization of objects and intensity required for trapping. Here we investigate a three-dimensional nanorod metamaterial platform, serving as an auxiliary tool for the optical manipulation, able to support and control near-field interactions and generate both steep and flat optical potential profiles. It was shown that the 'topological transition' from the elliptic to hyperbolic dispersion regime of the metamaterial, usually having a significant impact on various light-matter interaction processes, does not strongly affect the distribution of optical forces in the metamaterial. This effect is explained by the predominant near-fields contributions of the nanostructure to optomechanical interactions. Semi-analytical model, approximating the finite size nanoparticle by a point dipole and neglecting the mutual re-scattering between the particle and nanorod array, was found to be in a good agreement with full-wave numerical simulation. In-plane (perpendicular to the rods) trapping regime, saddle equilibrium points and optical puling forces (directed along the rods towards the light source), acting on a particle situated inside or at the nearby the metamaterial, were found.

The ability to control mechanical motion of micro- and nano-scale particles with focused laser beams is an essential tool, being a paramount for a wide range of applications, related to bio-physics, micro-fluidics, optomechanical devices and more[1–4]. Being first proposed and demonstrated by A. Ashkin[5], the classical optical tweezers are nowadays a rapidly developing area of fundamental and applied research.

One of the promising and already conceptually proven approaches for improving performances of the optical manipulation schemes is to employ various auxiliary nanostructures, especially plasmonic ones[1,6]. The key idea of the plasmonic tweezers is to utilize strong light-matter interaction between nanostructured metals and focused laser beams. Noble metals, having a negative permittivity in the optical and infrared spectral ranges, support localized plasmon resonances enabling enhancement and control of near-fields at their vicinity[7,8]. In particular, the creation of strong intensity gradients is beneficial for obtaining substantial optical forces, which is important, for example, for achieving molecular manipulation[9]. Resonant amplification of optical forces, exceeding the amplification in plasmonic structures, can be achieved in all-dielectric planar metamaterials due to Fano resonances[10].

Plasmonic nanostructures with subwavelength light concentration could be employed for obtaining new optomechanical effects, i.e. accelerating nanoparticles in an arbitrary direction (in relation to the light propagation direction)[11], or for creating nano-modulators of plasmonic signals[12].

Arrays of antennas and their integrations in photonic circuitry[1,13], employed as auxiliary tools for optical trapping, were shown to outperform classical schemes (focused lasers in homogeneous media, e.g. liquid solutions) both in terms of spatial localization and optical power required per trapped particle. Antenna arrays were further extended for multifunctional platforms, enabling trapping, stacking, and sorting[14]. However, isolated plasmonic structures create limited number of hot spots (local enhancement of intensity) and are usually restricted to two-dimensional geometries. These constrains set significant

[1]ITMO University, St. Petersburg, 197101, Russia. [2]Ioffe Institute, St. Petersburg, 194021, Russia. [3]Peter the Great St. Petersburg Polytechnic University, St. Petersburg, 195251, Russia. [4]School of Electrical Engineering, Tel Aviv University, Tel Aviv, 69978, Israel. Correspondence and requests for materials should be addressed to A.A.B. (email: bogdanov@mail.ioffe.ru)

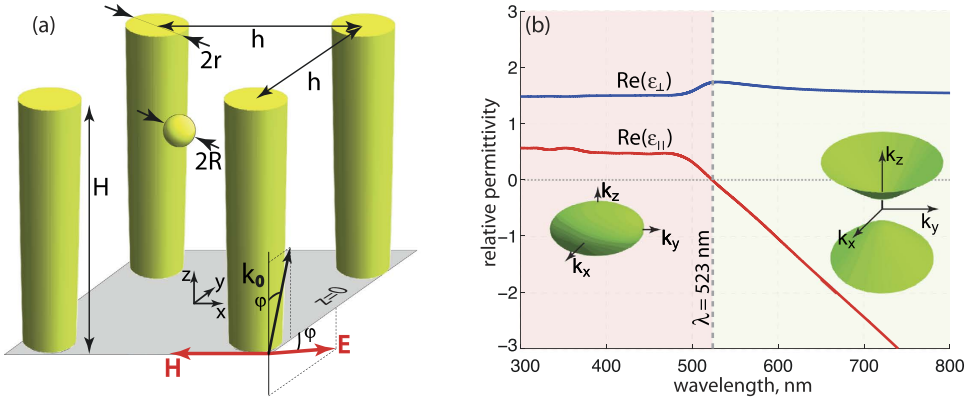

Figure 1. (**a**) Schematics of the nanorod metamaterial with a spherical nanoparticle inside. Radius of the nanoparticle is $R = 5$ nm. Height and radius of the nanorods are $H = 350$ nm and $r = 15$ nm, respectively, the period is $h = 60$ nm. (**b**) Frequency dependence of the effective tensor components (real parts) of the nanorod metamaterial. Dashed line shows the transition between elliptic and hyperbolic dispersion regimes of the metamaterial – epsilon-near-zero (ENZ) point. Insets show characteristic shapes of iso-frequency surfaces, corresponding to the dispersion regimes.

limitations on the flexibility of optical manipulation by reducing potential degrees of freedom, available for optomechanical control. On the other hand, three-dimensional artificially created nanostructures or metamaterials could provide additional benefits and flexibility by configuring near-field interactions in large volumes[15].

Hyperbolic metamaterials[16] are one class of artificially created electromagnetic structures, capable to enhance efficiencies of various light-matter interaction processes owning to the unusual dispersion regimes of eigenmodes, supported by the structure – namely its hyperbolic dispersion. Among various possible designs of this type of metamaterials it is worth mentioning composites made of vertically aligned nanorods[17,18], periodic metal dielectric layers[19] and semiconductor quantum structures[20,21]. While the far-field interactions of waves with hyperbolic composites were proven to be well characterized in terms of the effective medium approximation, this description could be questioned if near-field mediated processes are involved[22].

The general criterion for estimating impact of near-field contributions to an interaction is based on comparison of k-vector spectra with reciprocal vector of the metamaterial lattice. For example, scattering from objects within hyperbolic metamaterials involves consideration of the near-field effects[23].

Analysis of near- and far-field contributions to optical force, acting on objects embedded in the nanorod metamaterial is the central topic of the manuscript. In particular, optical forces, acting on nano-sized spherical particle embedded inside the metamaterial assembly, are investigated both numerically and by using a semi-analytical approach, considering the finite size nanoparticle as a point dipole and neglecting re-scattering between the particle and nanorod array. The impact of the finite structure of the metamaterial unit cell and the relative arrangement of the particle in respect to it was analyzed as a function of the system's geometry and frequency of incident illumination. A semi-analytical approach based on dipole near-field interaction is developed and shown to be in a good agreement with results of the full-wave numerical analysis. The interplay between near- and far-field effects in the context of effective medium approximation is discussed.

Nanorod Metamaterial: far-field characteristics

The geometry under investigation is schematically represented in Fig. 1a – it shows an array of vertically aligned gold nanorods and a gold nanoparticle placed inside it. Material parameters of the constitutive elements were taken from widely used sources[24]. The parameters of the structure are indicated in the figure caption. While the nanorods in this model are situated in vacuum, substrate effects and host material filling the space between the rods could be taken into account straightforwardly. Similar structures have already found use in various multidisciplinary applications, among them bio-sensing[25], enhancement of nonlinearities[26], acoustic waves detection[27], thin optical elements[18] and others. The key properties of this auxiliary nanostructure leading to enhanced performance are large surface area and unusual collective optical response of the system, enabling control over both far- and near-field interactions. Hence, investigation of optical forces, mediated by nanorod metamaterials, has a profound potential interest.

Far-field interactions between electromagnetic waves and metamaterials, under certain circumstances, can be described within the effective medium approximation. The main idea of this homogenization procedure is to average the electromagnetic field over a unit cell of a structure. Therefore, the field inside the structure is assumed to be uniform. In the context of optical forces, as it will appear in the next section, the non-uniformities play a major role and, in fact, predefine the spatial structure of optical potentials.

Recently, a phenomenological approach taking into account the finite size of the metamaterial unit cell was proposed[28]. Inclusion of a depolarization volume around optically manipulated particles enabled investigations of far-field contributions to optical forces. However, near-field interactions, being strongly dependent on a specific metamaterial design, were not included explicitly.

One of the key properties of hyperbolic metamaterials, making them attractive for electromagnetic applications, is their unique ability to support an unusual regime of dispersion caused by having permittivity tensor components of opposite signs ($\varepsilon_\perp \varepsilon_\parallel < 0$). An immediate implication of this hyperbolic dispersion regime is the high density of photonic states, available for both emission and scattering[29,30].

The effective permittivity tensor of nanorod metamaterial is given by:

$$\varepsilon = \begin{pmatrix} \varepsilon_\perp & 0 & 0 \\ 0 & \varepsilon_\perp & 0 \\ 0 & 0 & \varepsilon_\parallel \end{pmatrix}. \quad (1)$$

Here $\varepsilon_\perp$ and $\varepsilon_\parallel$ are effective permittivities perpendicular and along the wires, respectively.

Dispersion of the tensor components for the structure under consideration was calculated with the approach developed in[31]. The transition between elliptic and hyperbolic dispersion regimes occurs at the wavelength around 523 nm (see Fig. 1b). The transition point is called epsilon-near-zero (ENZ) regime, as the real part of the permittivity along the rods is vanishing, if the spatial dispersion effects are ignored. The high density of photonic states as well as the strong scattering emerges in the hyperbolic and ENZ regimes. The wavelength of the external illumination, exploited for optical manipulation in the subsequent investigations, is chosen around this ENZ point in order to distinguish between various dispersion regimes and their impact on optical forces.

Optical force distribution

Numerical model. The distribution of the optical forces, acting on the gold nanoparticle placed inside the wire medium is analyzed hereafter. The hyperbolic, ENZ, and elliptic dispersion regimes of the bulk metamaterial and their impacts on optical forces are compared and discussed.

In the first case, normal incidence scenario is considered – the illumination is chosen to be linearly polarized along the y-axis and it propagates along the z-axis ($\varphi = 0°$, see Fig. 1a). Oblique incidence with $\varphi = 45°$ will be investigated hereafter. Full 3D numerical analysis, based on finite elements method[32], is performed in order to calculate self-consistent electromagnetic fields in the system. Consequently, optical forces acting on the nanoparticle are calculated by integrating the Maxwell's stress tensor components over an imaginary spherical surface surrounding the nanoparticle.

The presence of a single nanoparticle breaks the inherent translation symmetry of the initial metamaterial geometry. In order to overcome the computation complexity of large systems modeling, Floquet periodical boundary conditions were imposed on finite size geometries. This type of model corresponds to a periodic system with variable unit cell, which consists of a square array of nanorods and the nanoparticle. If the electromagnetic coupling between the particles in adjacent cells is minor, this type of analysis recovers the behavior of the infinite system with a single particle.

The numerical procedure is as follows: the number of rods in the unit cell is increased gradually and the convergence of a certain quantity (optical forces in our case) is checked. Recently, a similar approach was applied in studies of the Purcell effect in nanorod[33] and wire[34] metamaterials. Square unit cells containing 4, 9, and 16 nanorods were considered and the convergence of optical force values at different points of the metamaterial volume was checked. A unit cell of 4 nanorods (the smallest one) was shown to predict the behavior of an infinite array within the accuracy of several percent. All the subsequent results were obtained for this size of the unit cell. The direct consequence of this calculation is that (i) only nearest neighbor rods define the value of optical force and (ii) nanoparticles in different unit cells almostly do not interact with each other.

It should be noted, however, that the collective macroscopic behavior of the array is taken into account by imposing periodical Floquet boundary conditions.

Lateral force component. All the subsequent calculations were done for a particle of 10 nm in diameter. The optical force $\mathbf{F}$, in the most general case, has three non-zero components (F_x, F_y, F_z). The lateral force $\mathbf{F}_\perp = (F_x, F_y, 0)$ will be analyzed first. Values of optical forces are normalized to the intensity of the incident wave and volume of the particle in order to perform direct comparisons with other optical manipulation schemes.

The resulting normalized forces at the cut-plane z = 10 nm, calculated for wavelengths $\lambda = 450$ and 600 nm, corresponding to the elliptic and hyperbolic dispersion regimes respectively, are shown in Fig. 2(a). Numerical simulation shows that spatial distribution of both electric field and optical force for different wavelengths of excitation (different dispersion regimes) are qualitatively similar and the quantitative difference is shown with different color bars on top panel in Fig. 2. The qualitative explanation of such a behavior is two fold: (i) small size of the sphere and nanorods (in comparison with wavelength) enables considering those structures as point dipoles; (ii) the same material of the sphere and nanorods providing similar frequency behaviour of their polarizability.

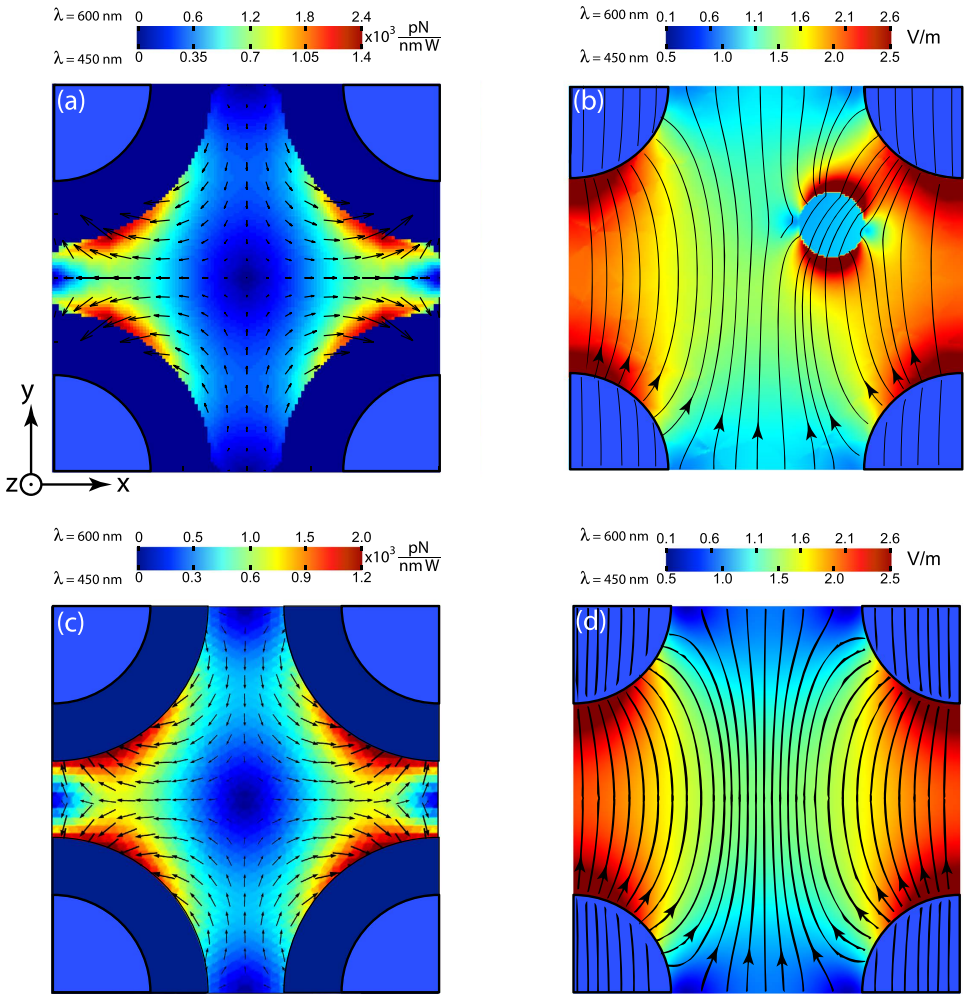

Figure 2. (**a**) Lateral optical force distribution at the cut-plane $z = 10$ nm [see Fig. 1(a)]. Magnitude of the lateral force $\mathbf{F}_{\parallel} = (F_x, F_y, 0)$ is shown with a color scale and the direction with arrows. (**b**) Distribution of the electric field magnitude in the cut-plane $z = 10$ nm. Magnitude of the electric field is shown with the color scale. The arrow lines are electric field lines. Panel (**c**) shows the distribution of the force calculated with a semi-analytical dipolar approach [see Eq. (2)], i.e. where the perturbation of the field by the particle is neglected. Panel (**d**) shows the numerical simulation of the electric field magnitude distribution without the particle. Panel (**a**) should be compared with (**c**), while (**b**) with (**d**). Dark blue shells around nanorods on panels (**a**), (**c**) have the width equal to particle's radius. Optical forces are not calculated at those areas, as the nanoparticle's center cannot approach the nanorods that close. Upper and lower scales of the color bars correspond to the hyperbolic ($\lambda = 600$ nm) and elliptic ($\lambda = 450$ nm) dispersion regimes of the metamaterial, respectively. Electric field amplitude of the incident wave is 1 V/m. Electric field **E** of the incident wave is parallel to the y-axis. Wavevector of the incident wave $\mathbf{k} = (0, 0, k_0)$.

Force maps at various cut-planes (with different z-coordinate) show qualitatively similar behavior too. The reasoning is as follows: at normal incidence, lateral optical force is mainly determined by first (gradient) term in Eq. (2). Within a good approximation $|\mathbf{E}|^2$ can be factorized as $f(z)g(x, y)$, where $f(z)$ is Fabry-Perot envelope function and $g(x, y)$ is the in-plane field distribution. Therefore, the lateral force distribution is similar for different cut-planes while its absolute value is modulated by Fabry-Perot envelope function.

It should be noted, that the values and directions of forces are attributed to the geometrical center of the particle, hence certain regions (dark blue shells around nanowires with thickness equal to the radius of nanoparticle) on Fig. 2(a,c) are blank, as this center cannot approach the boundaries of the rods.

It can be seen from Fig. 2(a) that the force distribution has saddle points at the center of the unit cell and at its edges between the rods. These places correspond to the the saddle points of electromagnetic field magnitude distribution [Fig. 2(d)], and, consequently, to the unstable equilibrium positions of the nanoparticle. Some peculiarities in the optical force distribution appear on cut-planes near the edges of the nanorods ($z = 350$ nm and $z = 0$ nm), but they are attributed to the longitudinal (z-component) force component and will be discussed further.

The similarity of the spatial distribution of the forces at hyperbolic and elliptic dispersion regimes results from the dominating near-field coupling between the nanorods and the particle. Figure 2(b) shows the magnitude distribution of total electric field $|\mathbf{E}| = \left(E_x^2 + E_y^2 + E_z^2\right)^{1/2}$, while the arrows show its direction. One can see that the field map is formed by electrical dipoles induced on the rods and the particle by the incident wave. Orientations of the dipoles nearly coincide with the polarization of the incident wave. Minor deviations from the above description are related to the higher multipole contribution and the interaction between the particle and the nanorods.

Lateral force distribution analysis can be provided with the following semi-analytical approach. First, the total electric field distribution in the nanorod array under external incident wave without the particle is calculated numerically with the periodic boundary conditions applied. Results of the simulation are shown in Fig. 2(d). The knowledge of the spatial distribution of the electric field magnitude enables calculation of optical forces with two assumptions: (i) the nanoparticle is represented by a structureless point electric dipole with a moment $\boldsymbol{\mu}$ (ii) the dipole is assumed to act as a small perturbation to the fields of the standalone metamaterial. This means, that only collective scattering properties of the nanorod array were taken into account, while the mutual re-scattering of the field between the particle and nanorods was neglected. Comparison between Fig. 2(b,d) verifies this approximation – both the structure and values of the field magnitude are similar.

The time averaged optical force acting on the point dipole is given by[7]:

$$\langle \mathbf{F} \rangle = \frac{\alpha'}{4}\nabla|\mathbf{E}|^2 + \frac{\alpha''}{2}\frac{\omega}{c}\sqrt{\frac{\mu_0}{\varepsilon_0}}\,\mathrm{Re}[\mathbf{E} \times \mathbf{H}^*], \tag{2}$$

where $\alpha = \alpha' + i\alpha''$ is the complex particle's polarizability. The polarizability of the spherical particle is given by[7]:

$$\alpha = 4\pi\varepsilon_0 R^3 \frac{\varepsilon_{\mathrm{Au}} - 1}{\varepsilon_{\mathrm{Au}} + 2}. \tag{3}$$

The resulting optical force map, calculated using the dipolar approximation [Eq. (2)] appears on Fig. 2(c). The arrows show the direction of the force at corresponding points. The color pattern corresponds to the absolute value of the force. The remarkable similarities between Maxwell's stress tensor calculations [Fig. 2(a)] and the approximate analytical model [Fig. 2(c)] suggest the validity of the dipolar model and highlights the impact of near-fields on the optical force. It should be noted, however, that overall values of optical forces, calculated within those approaches, have about 20% difference, which is related to the finite size of the particle and the mutual field re-scattering between the particle and nanorods.

Distribution of optical force in the case of oblique incidence ($\varphi = 45°$, see Fig. 1a) obtained with full numerical simulations and semi-analytical approach is shown in Fig. 3. One can see that in contrast to the case of normal incidence electric field distribution around the nanorods is asymmetric [Fig. 3(b,d)]. It results in asymmetry of optical force distribution. The asymmetry can be explained by excitation of non-dipole modes in the nanorods at oblique illumination[35].

Vertical force component. The distribution of the lateral optical force component (perpendicular to the nanorods) was analyzed in the previous section. Longitudinal force component F_z (parallel to the nanorods) is analyzed here.

As it was already mentioned, the homogenization procedure averages the near-fields over the unit cell, hence, it is inapplicable for estimation of gradient optical force in the lateral plane. Nevertheless, the field distribution along the z-axis can be roughly estimated considering the slab of the nanorod metamaterial as a Fabry-Perot resonator in z-direction[33]. Therefore, it is reasonable to expect a standing wave in the slab (along the z-axis) and maxima of the electric field resulting in in-plain trapping of the particle. The results of the numerical calculation suggest the validity of this hypothesis. Estimation of the field maxima position deeply inside the slab can be provided by the effective medium approximation[36,37] but a more detailed analysis, that takes into account boundary effects, demands numerical simulation.

The profiles of the total electric field magnitude along the line parallel to the rods and passing through the point $x = 30$ nm and $y = 5$ nm [see inset in Fig. 4(a)] calculated without nanoparticle for the elliptic ($\lambda = 450$ nm), ENZ ($\lambda = 523$ nm), and hyperbolic ($\lambda = 600$ nm) regimes are shown in Fig. 4(a). The insets show distribution of the total electric field magnitude in xz-plane passing through $y = 5$ nm. One can see that electric field distribution along the z-axis strongly depends on the wavelength of the incident wave. In the hyperbolic regime ($\lambda = 600$ nm), three distinct field maxima are observed – one inside the slab and two in the vicinity of its boundaries. In the elliptic ($\lambda = 450$ nm) and ENZ ($\lambda = 523$ nm) regimes, field decays inside the metamaterial and weak oscillations do not possess sharp field maxima. Additional contribution to those differences (apart from the interplay of dispersion regime and geometry, namely Fabry-Perot conditions) comes from a strong wavelength dependence of losses in gold[24]:

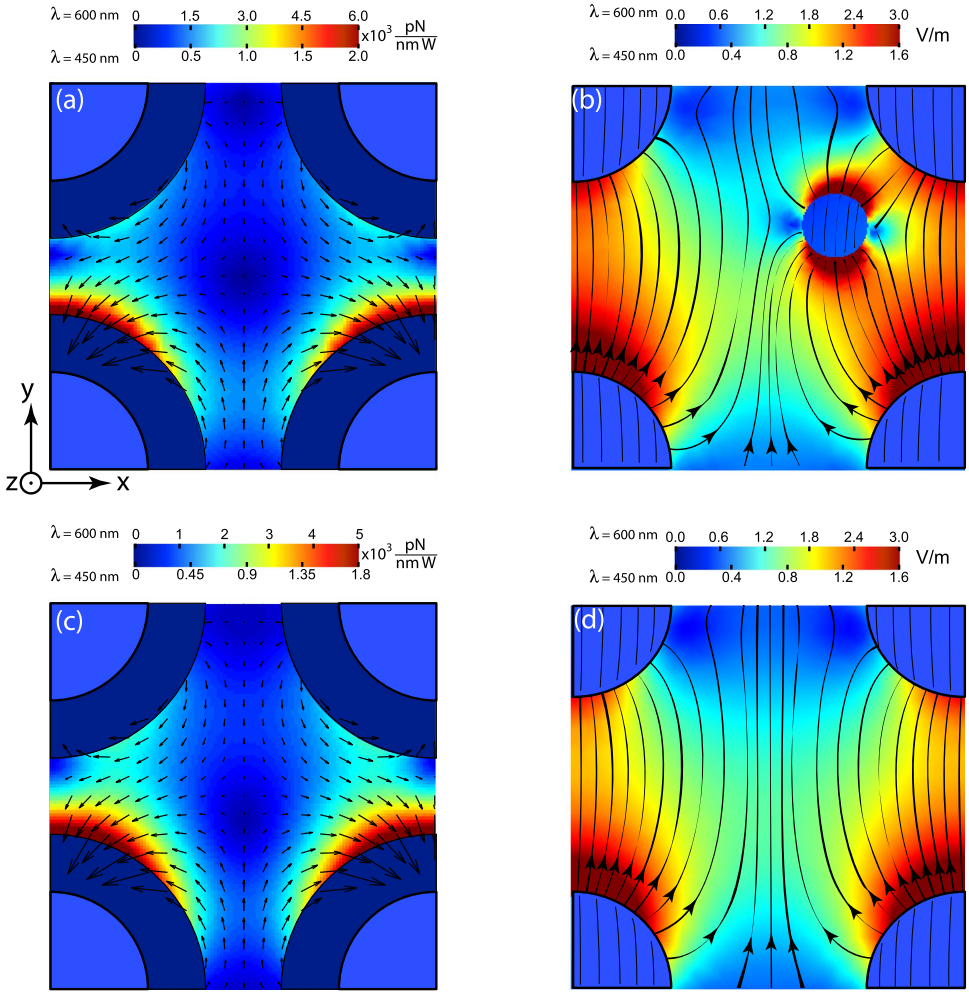

Figure 3. (**a**) Lateral optical force distribution at the cut-plane $z = 10$ nm see Fig. 1(a)]. Magnitude of the lateral force $\mathbf{k} = (0, k_0/\sqrt{2}, k_0/\sqrt{2})$ is shown with a color scale and the direction with arrows. (**b**) Distribution of the electric field magnitude in the cut-plane $z = 10$ nm. Magnitude of the electric field is shown with the color scale. The arrow lines are electric field lines. Panel (**c**) shows the distribution of the force calculated with a semi-analytical dipolar approach [see Eq. (2)], i.e. where the perturbation of the field by the particle is neglected. Panel (**d**) shows the numerical simulation of the electric field magnitude distribution without the particle. Panel (**a**) should be compared with (**c**), while (**b**) with (**d**). Dark blue shells around nanorods on panels (**a**), (**c**) have the width equal to particle's radius. Optical forces are not calculated at those areas, as the nanoparticle's center cannot approach the nanorods that close. Upper and lower scales of the color bars correspond to the hyperbolic ($\lambda = 600$ nm) and elliptic ($\lambda = 450$ nm) dispersion regimes of the metamaterial, respectively. Electric field amplitude of the incident wave is 1 V/m. Electric field **E** of the incident wave lies in the zy-plane. Wavevector of the incident wave $\mathbf{k} = (0, k_0/\sqrt{2}, k_0/\sqrt{2})$.

$$\left|\frac{\mathrm{Re}(\varepsilon_{\mathrm{Au}})}{\mathrm{Im}(\varepsilon_{\mathrm{Au}})}\right| \approx \begin{cases} 0.3 & \text{for } \lambda = 450\,\mathrm{nm}; \\ 6.2 & \text{for } \lambda = 600\,\mathrm{nm}. \end{cases} \quad (4)$$

Optical losses cause the reduction in quality factors of the modes, smearing out the sharp peaks, as could be seen in the case of elliptic dispersion.

Distributions of the z-component of the optical force along the nanorod for elliptic ($\lambda = 450$ nm), ENZ ($\lambda = 523$ nm) and hyperbolic ($\lambda = 600$ nm) regimes are shown in Fig. 4(b). Positions of the stable trapping in transverse planes are marked with arrows (note, that the force derivative should be negative in order to obtain a stable equilibrium). Shaded areas on the figure show the regions within the metamaterial, where the optical force component F_z is directed towards the light source (for $\lambda = 600$ nm). Optical pulling forces or optical attraction gained considerable attention over the last decade, as it provides additional flexible degree of freedom in optical manipulation[38].

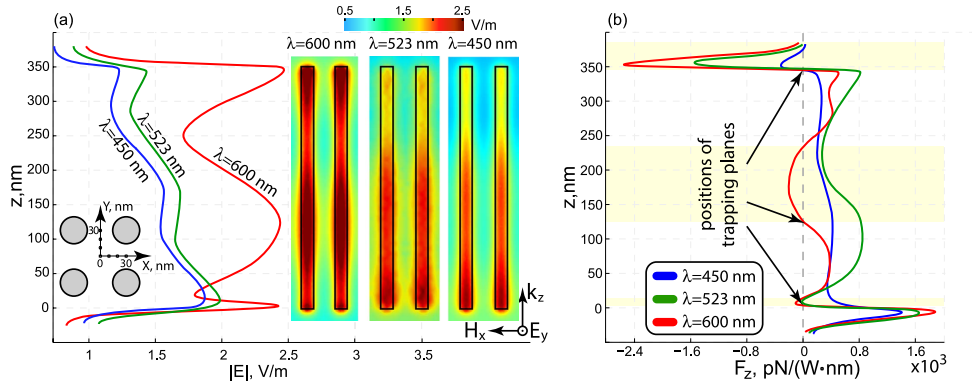

Figure 4. Distribution of: (**a**) Total electric field magnitude |E| and (**b**) longitudinal optical force component F_z along the line passing through the point with coordinates $x = 30$ nm and $y = 5$ nm (see the inset with geometrical arrangement) and parallel to the nanorods for the elliptic ($\lambda = 450$ nm), ENZ ($\boldsymbol{\lambda} = 523$ nm), and hyperbolic ($\lambda = 600$ nm) regimes of the metamaterial. The insets in panel (**a**) show the distribution of the electric field magnitude in the *zx*-cut-plane passing through $y = 5$ nm for the elliptic ($\lambda = 450$ nm), ENZ ($\lambda = 523$ nm), and hyperbolic ($\lambda = 600$ nm) regimes of the metamaterial. Shaded areas in panel (**b**) show the region where a pulling force emerges. Electric field amplitude of the incident wave is 1 V/m.

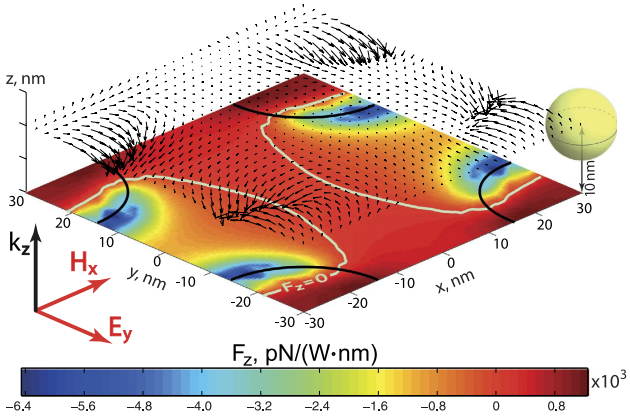

Figure 5. Distribution of the normalized optical force acting on the nanoparticle, situated at the lateral plane above the metamaterial. Distance between the center of the nanoparticle and top faces of the nanorods is 10 nm. Arrows show the direction of the optical force. Color map shows the distribution of the optical force component parallel to the nanorods (F_z). Black solid lines show the the geometrical edges of the nanorods.

The hyperbolic regime supports three regions of optical attraction, while the elliptic and ENZ have only one, as could be seen in Fig. 4(b). This occurrence could be understood as follows: in the elliptic regime both weak gradient of the electric field magnitude [see Fig. 4(a)] and high material losses of the particle result in the domination of radiation pressure [second term in Eq. (2)] over the gradient force. The radiation pressure is co-directional with the Poynting vector of the incident radiation, so the optical attraction cannot be obtained in this case. Nevertheless, the first term of Eq. (2) overcomes the second one in the vicinity of the nanorod's edge where strong gradient of the electric field intensity is observed [see Fig. 4(a)]. In the hyperbolic regime, on the other hand, there are several regions where the optical force component is directed to the light source – that's the result of high quality factor Fabry-Perot modes and dominating real part of the particle's polarizability.

For the hyperbolic regime ($\lambda = 600$ nm), optical potential in the vicinity of nanorod's edge is stronger than in elliptical and ENZ regimes. For example, optical traping potential of 26 meV for 5nm radius particle can be achieved with electric field intensity ~10^7 V/m that corresponds to focusing of 1 W beam to 3 μm spot in diameter.

As a separate case, the particle situated over the metamaterial slab will be considered next. This scenario describes the case where the metamaterial is used as a substrate for advanced optical manipulation. Results of numerical studies appear in Fig. 5, showing the distribution of the vertical optical force acting on the nanoparticle in the lateral plane of $z = 10$ nm above the nanorods. It could be seen, that

the maximal attraction force on the particle emerges in the vicinity of nanorods edges (the sample is illuminated from below – see Fig. 5). Arrows indicate the direction of the optical force. Color pattern shows the distribution of the optical force component parallel to the nanorods (F_z). Solid white lines correspond to $F_z = 0$. Remarkable behaviour of forces above the metamaterial substrate could suggest the later as an auxiliary nanostructure or metasurface, providing additional flexibility in optical manipulation.

Conclusion

In this work, comprehensive analysis of the optical forces acting on a metal nanoparticle placed inside or in the vicinity of three-dimensional nanorod metamaterial slab was performed. Numerical simulations of finite size square unit cells with periodical Floquet boundary conditions enable to take into account all collective effects in the metamaterial and estimate optical forces on small particles. Unit cells containing 4, 9, and 16 nanorods were analyzed and the convergence of the optical forces for different positions of the particle was checked. It was shown that the smallest unit cell already reproduces the effect of optical forces on a particle, situated within the infinite metamaterial. Therefore, only four neighboring nanorods nearest to the particle make the dominant contribution to the optical forces. This statement has been confirmed with the developed semi-analytical model which neglects the particle's interior and the re-scattering effects between the particle and nanorods. Furthermore, it was shown that the 'topological transition' from the elliptic to hyperbolic dispersion regime of the metamaterial, usually having an impact on various light-matter interaction processes, is less important for optical forces.

In-plane optical trapping and optical pulling forces were observed. The comprehensive numerical modeling enables estimation of optical forces values, normalized to incident power and particle's volume. Values as high as 2.3×10^3 pN/W/nm for both lateral and optical pulling forces were predicted. Those results overcome other reported values[39,40].

The remarkable structure of predicted optomechanical interactions (in particular pulling forces), mediated by the metamaterial, makes the later to be a promising platform for large span of multidisciplinary applications, involving demands for precise nanoscale mechanical manipulation, including trapping sorting, mixing and more.

References

1. Juan, M. L., Righini, M. & Quidant, R. Plasmon nano-optical tweezers. *Nature Photonics* **5,** 349–356 (2011).
2. Dienerowitz, M., Mazilu, M. & Dholakia, K. Optical manipulation of nanoparticles: a review. *Journal of Nanophotonics* **2,** 021875 (2008). URL http://link.aip.org/link/JNOACQ/v2/i1/p021875/s1&Agg=doi.
3. Maragò, O. M., Jones, P. H., Gucciardi, P. G., Volpe, G. & Ferrari, A. C. Optical trapping and manipulation of nanostructures. *Nature Nanotechnology* **8,** 807–819 (2013).
4. Grier, D. G. A revolution in optical manipulation. *Nature* **424,** 810–816 (2003).
5. Ashkin, A. Acceleration and trapping of particles by radiation pressure. *Physical Review Letters* **24,** 156 (1970).
6. Zhang, J., MacDonald, K. F. & Zheludev, N. I. Optical gecko toe: Optically controlled attractive near-field forces between plasmonic metamaterials and dielectric or metal surfaces. *Physical Review B* **85,** 205123 (2012). URL http://link.aps.org/doi/10.1103/PhysRevB.85.205123.
7. Novotny, L. & Hecht, B. *Principles of nano-optics* (Cambridge university press, 2012).
8. Berkovitch, N., Ginzburg, P. & Orenstein, M. Nano-plasmonic antennas in the near infrared regime. *Journal of Physics: Condensed Matter* **24,** 073202 (2012).
9. Shoji, T. & Tsuboi, Y. Plasmonic optical tweezers toward molecular manipulation: Tailoring plasmonic nanostructure, light source, and resonant trapping. *The Journal of Physical Chemistry Letters* **5,** 2957–2967 (2014).
10. Zhang, J., MacDonald, K. F. & Zheludev, N. I. Giant optical forces in planar dielectric photonic metamaterials. *Optics Letters* **39,** 4883 (2014). URL http://www.ncbi.nlm.nih.gov/pubmed/25121899 https://www.osapublishing.org/ol/abstract.cfm?uri=ol-39-16-4883.
11. Shalin, A. S. & Sukhov, S. V. Plasmonic nanostructures as accelerators for nanoparticles: optical nanocannon. *Plasmonics* **8,** 625–629 (2013).
12. Shalin, A. S., Ginzburg, P., Belov, P. A., Kivshar, Y. S. & Zayats, A. V. Nano-opto-mechanical effects in plasmonic waveguides. *Laser & Photonics Reviews* **8,** 131–136 (2014).
13. Lin, P.-T., Chu, H.-Y., Lu, T.-W. & Lee, P.-T. Trapping particles using waveguide-coupled gold bowtie plasmonic tweezers. *Lab on a Chip* **14,** 4647–4652 (2014).
14. Roxworthy, B. J. *et al.* Application of plasmonic bowtie nanoantenna arrays for optical trapping, stacking, and sorting, *Nano Letters* **12,** 796–801 (2012).
15. Cai, W. & Shalaev, V. *Optical metamaterials: fundamentals and applications* (Springer, 2010).
16. Shekhar, P., Atkinson, J. & Jacob, Z. Hyperbolic metamaterials: fundamentals and applications. *Nano Convergence* **1,** 1–17 (2014).
17. Atkinson, R. *et al.* Anisotropic optical properties of arrays of gold nanorods embedded in alumina. *Physical Review B* **73,** 235402 (2006).
18. Ginzburg, P. *et al.* Manipulating polarization of light with ultrathin epsilon-near-zero metamaterials. *Optics Express* **21,** 14907–14917 (2013).
19. Krishnamoorthy, H. N., Jacob, Z., Narimanov, E., Kretzschmar, I. & Menon, V. M. Topological transitions in metamaterials. *Science* **336,** 205–209 (2012).
20. Hoffman, A. J. *et al.* Negative refraction in semiconductor metamaterials. *Nature Materials* **6,** 946–950 (2007).
21. Ginzburg, P. & Orenstein, M. Nonmetallic left-handed material based on negative-positive anisotropy in low-dimensional quantum structures. *Journal of Applied Physics* **103,** 083105 (2008).
22. Ginzburg, P. *et al.* Self-induced torque in hyperbolic metamaterials. *Physical Review Letters* **111,** 036804 (2013).
23. Shalin, A. S. *et al.* Scattering suppression from arbitrary objects in spatially dispersive layered metamaterials. *Phys. Rev. B* **91,** 125426 (2015). URL http://link.aps.org/doi/10.1103/PhysRevB.91.125426.
24. Johnson, P. B. & Christy, R. W. Optical Constants of the Noble Metals. *Physical Review B* **6,** 4370 (1972). URL http://dx.doi.org/10.1103/PhysRevB.6.4370.
25. Kabashin, A. *et al.* Plasmonic nanorod metamaterials for biosensing. *Nature Materials* **8,** 867–871 (2009).

26. Wurtz, G. A. *et al.* Designed ultrafast optical nonlinearity in a plasmonic nanorod metamaterial enhanced by nonlocality. *Nature Nanotechnology* **6,** 107–111 (2011).
27. Yakovlev, V. V. *et al.* Ultrasensitive non-resonant detection of ultrasound with plasmonic metamaterials. *Advanced Materials* **25,** 2351–2356 (2013).
28. Shalin, A., Sukhov, S., Bogdanov, A., Belov, P. & Ginzburg, P. Optical pulling forces in hyperbolic metamaterials. *Phys. Rev. A* (2015).
29. Jacob, Z. *et al.* Engineering photonic density of states using metamaterials. *Applied Physics B* **100,** 215–218 (2010).
30. Iorsh, I. V., Poddubny, A. N., Ginzburg, P., Belov, P. A. & Kivshar, Y. S. Compton-like polariton scattering in hyperbolic metamaterials. *Physical Review Letters* **114,** 185501 (2015).
31. Elser, J., Wangberg, R., Podolskiy, V. A. & Narimanov, E. E. Nanowire metamaterials with extreme optical anisotropy, *Applied Physics Letters* **89,** 261102 (2006). URL http://scitation.aip.org/content/aip/journal/apl/89/26/10.1063/1.2422893.
32. Pryor, R. W. *Multiphysics Modeling Using COMSOL* (Jones & Bartlett Learning, 2011).
33. Slobozhanyuk, A. P. *et al.* Purcell effect in hyperbolic metamaterial resonators, *arXiv preprint arXiv:1504.06950* (2015).
34. Mirmoosa, M., Kosulnikov, S. Y. & Simovski, C. Topological phase transition in wire medium enables high purcell factor at infrared frequencies, *arXiv preprint arXiv:1504.05936* (2015).
35. Velichko, E. A. & Nosich, A. I. Refractive-index sensitivities of hybrid surface-plasmon resonances for a core-shell circular silver nanotube sensor. *Optics Letters* **38,** 4978 (2013).
36. Silveirinha, M. G. Nonlocal homogenization model for a periodic array of ε-negative rods. *Physical Review E* **73,** 046612 (2006). URL http://link.aps.org/doi/10.1103/PhysRevE.73.046612.
37. Tyshetskiy, Y. *et al.* Guided modes in a spatially dispersive wire medium slab. *JOSA B* **31,** 1753–1760 (2014).
38. Chen, J., Ng, J., Lin, Z. & Chan, C. Optical pulling force. *Nature Photonics* **5,** 531–534 (2011).
39. Yang, X., Liu, Y., Oulton, R. F., Yin, X. & Zhang, X. Optical forces in hybrid plasmonic waveguides. *Nano Letters* **11,** 321–328 (2011).
40. Wang, K., Schonbrun, E. & Crozier, K. B. Propulsion of gold nanoparticles with surface plasmon polaritons: Evidence of enhanced optical force from near-field coupling between gold particle and gold film. *Nano Letters* **9,** 2623–2629 (2009).

Acknowledgements

This work was partially supported by the Government of the Russian Federation (Grant 074-U01), by the Russian Foundation for Basic Research (No. 15-02-01344), by the Program on Fundamental Research in Nanotechnology and Nanomaterials of the Presidium of the Russian Academy of Sciences. The investigation of optical forces distributions has been supported by the Russian Science Foundation Grant No. 14-12-01227. A.B. thanks Russian Federation President support program of leading scientific schools (NSh-5062.2014.2) and RFBR (No. 14-02-01223).

Author Contributions

A.B. performed the numerical simulations. A.S. supervised the project. The paper was written by A.B. and P.G. All authors discussed the results and contributed to the manuscript.

Additional Information

Competing financial interests: The authors declare no competing financial interests.

How to cite this article: Bogdanov, A. A. *et al.* Optical forces in nanorod metamaterial. *Sci. Rep.* **5**, 15846; doi: 10.1038/srep15846 (2015).